ADVANCED ENERGY MATERIALS
www.advenergymat.de

Rationally Designed Hierarchical TiO_2@Fe_2O_3 Hollow Nanostructures for Improved Lithium Ion Storage

*Jingshan Luo, Xinhui Xia, Yongsong Luo, Cao Guan, Jilei Liu, Xiaoying Qi, Chin Fan Ng, Ting Yu, Hua Zhang, and Hong Jin Fan**

Hollow and hierarchical nanostructures have received wide attention in new-generation, high-performance, lithium ion battery (LIB) applications. Both TiO_2 and Fe_2O_3 are under current investigation because of their high structural stability (TiO_2) and high capacity (Fe_2O_3), and their low cost. Here, we demonstrate a simple strategy for the fabrication of hierarchical hollow TiO_2@Fe_2O_3 nanostructures for the application as LIB anodes. Using atomic layer deposition (ALD) and sacrificial template-assisted hydrolysis, the resulting nanostructure combines a large surface area with a hollow interior and robust structure. As a result, such rationally designed LIB anodes exhibit a high reversible capacity (initial value 840 mAh g^{-1}), improved cycle stability (530 mAh g^{-1} after 200 cycles at the current density of 200 mA g^{-1}), as well as outstanding rate capability. This ALD-assisted fabrication strategy can be extended to other hierarchical hollow metal oxide nanostructures for favorable applications in electrochemical and optoelectronic devices.

1. Introduction

Lithium ion batteries (LIBs) currently dominate the energy supply for portable electronics and show promising application in electric vehicles.[1,2] In addition, building large-scale, cabinet-type LIBs has provided a pathway to overcome the energy intermittency of renewable energy resources, such as wind and solar energy.[3,4] Thus, it is highly desirable to develop LIBs with high energy density and power density, long cycle life, and high rate capability to meet the increasing demand. Currently, commercial anodes are made of graphite. However, its energy density is low and using graphite imposes safety issues because of the lower operating voltage.[5,6] Over the past decades, a worldwide effort has been made to search for alternative anode materials for higher energy density and longer cycle life. Among the explored systems, transition metal oxides such as Co_3O_4,[7] NiO,[8] Fe_2O_3,[9] and SnO_2[10] have been considered as potential substitutes because of their higher reversible specific capacity (about three times larger than that of graphite).[11] In particular, Fe_2O_3 is one of the most promising anodes because of its high capacity, worldwide abundance, low cost, and non-toxic properties.[9,12–14] Despite of these attractive features, Fe_2O_3 shows a large volume expansion during the charge and discharge process which causes pulverization and deterioration of the active materials resulting in poor cyclability. Furthermore, the low conductivity of Fe_2O_3 hastens the degradation process especially at high current densities.[14–17]

Strategies to overcome the above drawbacks can be summarized into two main categories. The *first* strategy is to design various nanostructures,[11,18] such as nanoparticles,[19] nanowires,[7] and nanotubes,[9] because nanostructured electrodes can alleviate the strain caused by repeated Li insertion and extraction and avoid rapid capacity fading.[20,21] Among various nanostructures, hollow structures stand out because of several advantages, such as a short diffusion path for electron/ion transfer, a large electrode–electrolyte contact area, and interior free space to alleviate pulverization strain.[6,22,23] Template-assisted synthesis is one of the most widely used methods to prepare hollow nanostructures because it is a facile process that has great versatility. Previously, Liu et al. prepared Fe_2O_3 nanotubes using ZnO nanowires as the sacrificial template which showed good electrochemical performance in LIB applications.[16] The *second* approach relies largely on a judicious design of nanoarchitectures and smart hybridization of two active materials in synergy.[1,24,25] In this method, Fe_2O_3 particles are grafted onto either conductive and/or robust scaffolds to construct hybrid electrode materials. For example, metal nanowires,[1] carbon nanotubes,[26] and graphene[12,27] have been used as the conductive scaffold. TiO_2 is an excellent anode material with a relatively good conductivity and low volume expansion as a result of its layered crystalline structure. Therefore, it is possible to use it as the backbone of composite structures to alleviate the volume expansion and provide a highway for charge transfer.[5,28] Furthermore, TiO_2 is also abundant, low in cost and environmentally friendly, and it can attain a higher operation voltage (1.7 V vs. Li^+/Li), which makes it a safer material compared to graphite.[29–32]

J. S. Luo, Dr. X. H. Xia, Dr. Y. S. Luo, C. Guan, J. L. Liu, C. F. Ng, Prof. T. Yu, Prof. H. J. Fan
Division of Physics and Applied Physics
School of Physical and Mathematical Sciences
Nanyang Technological University
Singapore 637371, Singapore
E-mail: fanhj@ntu.edu.sg
Dr. X. Y. Qi, Prof. H. Zhang
School of Materials Science and Engineering
Nanyang Technological University
Singapore 639798, Singapore

DOI: 10.1002/aenm.201200953

The above two strategies could be realized with a one-electrode system. In this work, by employing atomic layer deposition (ALD) and liquid-phase self assembly, we have realized hierarchical hollow TiO_2@Fe_2O_3 core–shell nanoarrays. Nanowires of $Co_2(OH)_2CO_3$ on Ni foam serve as the sacrificial template for the subsequent formation of Fe_2O_3 nanospikes through an ion-exchange-accelerated hydrolysis. ALD-deposited TiO_2 is used as the backbone for the whole composite nanostructured electrode, in addition to its own capacity contribution. In such a rationally designed nanostructure electrode, the final Fe_2O_3 nanospikes have solid contact with the TiO_2 nanotube backbone, so that the former can provide the high capacity and the latter helps to retain the cyclic stability as well as to provide a pathway for direct charge transfer. Benefiting from the above advantages, the hierarchical hollow nanostructure LIB electrode exhibits high initial discharge and charge capacities, and an exceptionally stable capacity retention of 520 mAh g^{-1} after 200 cycles at a current density of 200 mA g^{-1}. Our work also demonstrates the usefulness of ALD in nanoscale energy materials.[33,34]

2. Results and Discussion

2.1. ALD-Assisted Nanofabrication and Characterization

The hierarchical hollow TiO_2@Fe_2O_3 core–shell nanostructure was prepared via a three-step method as illustrated in **Scheme 1**. First, a $Co_2(OH)_2CO_3$ nanowire array was prepared on Ni foam by a routine hydrothermal growth, which served as the sacrificial template. Second, a layer of TiO_2 with a thickness of about 10 nm was uniformly deposited on the surface of the $Co_2(OH)_2CO_3$ nanowire array by ALD. In the third step, the TiO_2-coated $Co_2(OH)_2CO_3$ nanowire array was bathed in 20 mM aqueous $FeCl_3$ solution at room temperature for 12 h. During this last process two things happen: Fe^{3+} slowly hydrolyzes at room temperature, resulting in FeOOH and H^+.[16] The H^+ ions can penetrate through the amorphous TiO_2 shell via diffusion and react with the core nanowire. Due to the solubility difference of $Co_2(OH)_2CO_3$ and FeOOH, the inner $Co_2(OH)_2CO_3$ core slowly dissolves. Simultaneously FeOOH precipitates are formed on the surface of the TiO_2 shell as nanospikes. After annealing in Ar atmosphere at 400 °C for 2 h, FeOOH was transformed into Fe_2O_3, and the amorphous TiO_2 shell crystallized, resulting in the hierarchical hollow TiO_2@Fe_2O_3 core–shell nanostructure. Unlike in previous work,[16] the TiO_2 middle layer in this method provides a scaffold for both the FeOOH precipitation and electron conduction path. This fabrication method is flexible. In fact, the core nanowire material is not limited to $Co_2(OH)_2CO_3$, but can be any oxide for example, ZnO, Al_2O_3 and MgO, as long as it can be etched by a weak acid generated by hydrolization of $FeCl_3$.

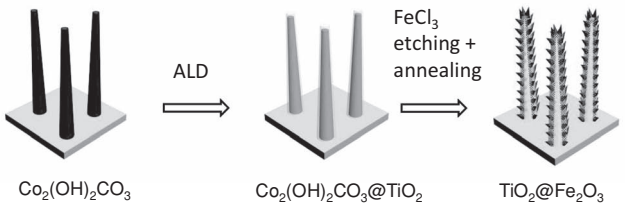

Scheme 1. Schematic illustration of the preparation process of a hierarchical hollow TiO_2@Fe_2O_3 core–shell nanostructures.

The crystal structure of TiO_2@Fe_2O_3 was determined by X-ray diffraction (XRD) analysis. To verify the compositional transformation, XRD patterns of the samples were recorded at different stages, as seen in **Figure 1**a. The hydrothermally grown nanowires were confirmed to be orthorhombic phase $Co(CO_3)_{0.5}(OH)0.11H_2O$ (JCPDS card no. 48-0083). After TiO_2 coating by ALD no new XRD peaks appeared, indicating the amorphous nature of TiO_2 which is in agreement with a previous report on low-temperature (120 °C) ALD of TiO_2.[35] After the $FeCl_3$ hydrolysis most of the peaks could be indexed to FeOOH, indicating that the as-obtained nanospikes are FeOOH. A weak peak due to $Co(CO_3)_{0.5}(OH)0.11H_2O$ was still detected at around 20°. This implies that a small amount of $Co(CO_3)_{0.5}(OH)0.11H_2O$ remains after the hydrolysis-induced etching. Energy-dispersive X-ray spectroscopy (EDS) also showed Co as a trace element (see Figure S2, Supporting Information). After annealing of the TiO_2@FeOOH core–shell hollow nanowires, only peaks related to anatase TiO_2 (JCPDS card no. 21-1272) and hematite Fe_2O_3 (JCPDS card no. 33-0664) were obtained in the XRD pattern, verifying the formation of the final TiO_2@Fe_2O_3 nanostructures.

To further characterize the composition of the final TiO_2@Fe_2O_3 nanostructure, X-ray photoelectron spectroscopy (XPS) was conducted. The result of the wide survey scan is shown in Figure S1 in the Supporting Information. Detailed scans of the Ti 2p range and the Fe 2p range are illustrated in Figure 1b and c, respectively. The two Ti 2p peaks centering at 460 and 466 eV stem from Ti $2p_{3/2}$ and Ti $2p_{1/2}$, respectively.[5] The splitting binding energy between the Ti $2p_{1/2}$ and Ti $2p_{3/2}$ core levels are 6 eV, indicating a normal state of Ti^{4+} in the anatase TiO_2. For the Fe 2p spectra, there are four peaks, Fe $2p_{2/3}$, Fe $2p_{1/2}$, and their satellites, centering at 711, 720, 725, and 734 eV, respectively, in accordance with the electronic state of α-Fe_2O_3.[36] No other peaks from Fe^{2+} were observed.

The morphology of the as-fabricated nanostructures was characterized by scanning electron microscopy (SEM) and transmission electron microscopy (TEM). It can be seen that the hydrothermally grown $Co_2(OH)_2CO_3$ nanowires have lengths of around 3 μm and diameters of around 150 nm, **Figure 2**a. After TiO_2 coating by ALD (thickness ca. 10 nm, see enlarged images in Figure S3, Supporting Information), there was no obvious morphology change due to the conformal characteristics of the ALD TiO_2 layer, Figure 2b. Figure 2c shows the final hierarchical hollow TiO_2@Fe_2O_3 core–shell nanowire array. The resulting Fe_2O_3 nanospikes were uniformly grafted on the surface of the TiO_2 scaffold, as is revealed in the enlarged SEM image, Figure 2d. **Figure 3**a shows the TEM image of a single $Co_2(OH)_2CO_3$ nanowire coated with TiO_2. Figure 3b clearly reveals that the interior of the final TiO_2@Fe_2O_3 nanostructure is hollow, and the Fe_2O_3 nanospikes are uniformly and closely together attached to the TiO_2 surface (more SEM images are provided in the Supporting Information, Figure S2). To show the crystallinity of the Fe_2O_3 spikes, HRTEM images were

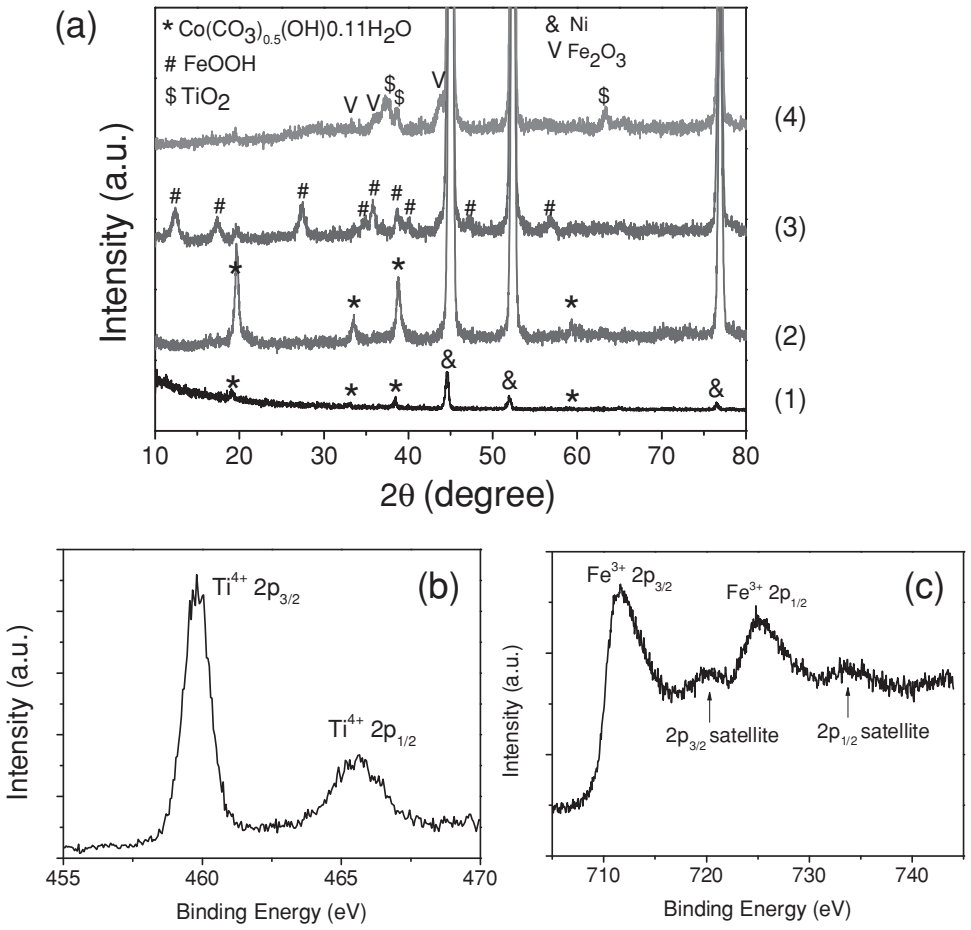

Figure 1. a) XRD spectra of the sample at different preparation stages: (1) Pristine nanowires, for which the exact phase is $Co(CO_3)_{0.5}(OH)0.11H_2O$; (2) after ALD TiO_2; (3) after $FeCl_3$ hydrolysis; and (4) final $TiO_2@Fe_2O_3$ core–shell nanostructures after thermal annealing. The three dominant peaks at around 45, 52, and 77° are from the Ni foam; b,c) XPS spectrum of the Ti 2p and Fe 2p regions of the $TiO_2@Fe_2O_3$ structure, respectively.

made of an individual nanospike, Figure 3c. We measured that the Fe_2O_3 spikes are polycrystalline and the lattice fringes of 0.27 nm match well with the inter-planar spacing of the (104) planes of α-Fe_2O_3.[37,38]

2.2. Application as Li-ion Battery Anode

Such a rationally designed electrode combines the advantages of being 'hollow' and 'open core–shell', both of which are expected to enhance the electrochemical performance for LIB applications. The hollow interior may help to alleviate the strain during Li insertion and extraction. The stable TiO_2 provides a robust structural support and transport pathway. To further increase the performance of the hybrid metal-oxide nanostructure as the electrode for LIB applications, a layer of amorphous carbon was coated on the surface of the $TiO_2@Fe_2O_3$ nanowire array by the commonly used glucose bath method.[16,39,40] This outer amorphous carbon layer makes the whole nanostructure more compact and conductive.

To evaluate the electrochemical performance of the $TiO_2@Fe_2O_3$ core–shell nanowire array as the anode for LIBs, standard coin-cells were assembled using a Li-metal circular foil as the counter electrode and 1 M $LiPF_6$ in ethylene carbonate and diethyl carbonate (1:1, v/v) as the electrolyte. The charge-storage behavior was first characterized by cyclic voltammetry (CV) using a scanning rate of 0.1 mV s^{-1}. **Figure 4**a shows the initial three representative CV curves of the discharge and charge processes. During the first discharge cycle, two well-defined reduction peaks were observed at 1.18 V and 0.58 V (vs. Li/Li^+), respectively. The peak at 1.18 V corresponds to the lithium intercalation into Fe_2O_3, $Fe_2O_3 + 2Li^+ + 2e^- \rightarrow Li_2(Fe_2O_3)$.[9,13,19,41] The second peak at 0.58 V is attributed to the further reduction of the $Li_2(Fe_2O_3)$ into Fe^0 and the formation of Li_2O, namely, $Li_2(Fe_2O_3) + 4Li^+ + 4e^- \rightarrow 2Fe^0 + 3Li_2O$.[13] During the anodic process of the first cycles, the peaks at 1.0, 1.58, and 2.2 V correspond to the multiple step oxidation of Fe^0.[9,19] Note that the cathodic peak at 1.2 V disappears in the subsequent cycles and the intensity of the peak at 0.88 V drops significantly compared to the first cycle, indicating the occurrence of some irreversible processes in the electrode material in the first cycle because of the formation of a solid electrolyte interphase (SEI) film. A pronounced reduction peak appears at 1.63 V in the subsequent cycles. This might be related to the lithium storage mechanism between tetragonal anatase TiO_2 and orthorhombic Li_xTiO_2 ($TiO_2 + xLi^+ + xe^- \leftrightarrow Li_xTiO_2$), as the anodic peak at 2.2 V might

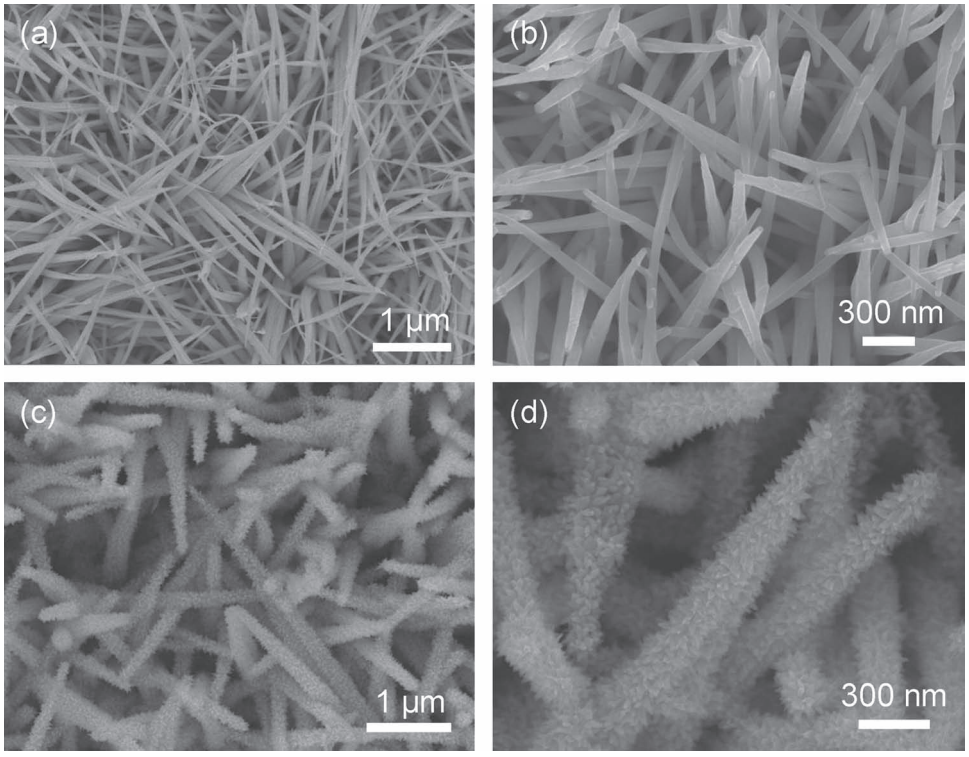

Figure 2. SEM images of the prepared samples. a) $Co_2(OH)_2CO_3$ nanowire array on Ni foam; b) TiO_2-coated $Co_2(OH)_2CO_3$ nanowire array; c,d) Low-magnification and high-magnification image, respectively, of the hierarchical hollow TiO_2@Fe_2O_3 core–shell nanostructure.

also be due to the oxidation of Li_xTiO_2.[28,29,32] It is worth noting that the CV peaks repeat themselves well during the subsequent cycles, indicating a good reversibility of the electrochemical reaction, and good cycling performance as discussed below.

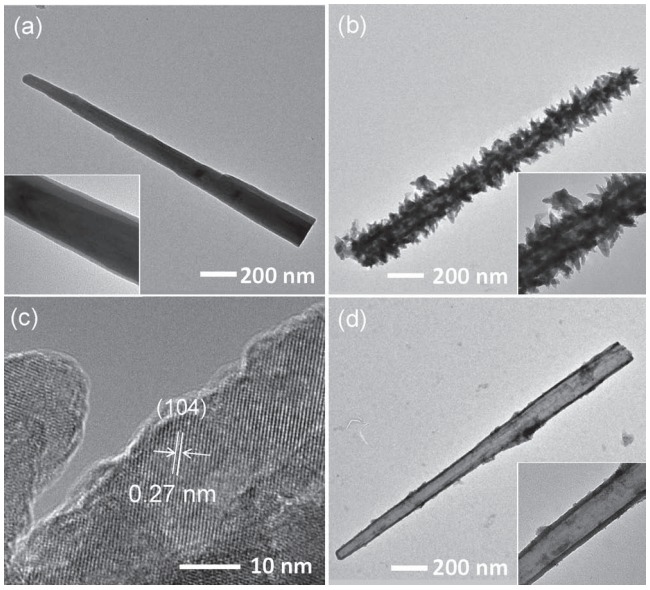

Figure 3. TEM and HRTEM of the prepared samples. a) TiO_2-coated $Co_2(OH)_2CO_3$ nanowire; b) hierarchical hollow TiO_2@Fe_2O_3 core–shell nanostructure; c) HRTEM image of an individual Fe_2O_3 nanospike; d) pure TiO_2 nanotube without Fe_2O_3.

In order to evaluate the cycle stability of the electrodes, the discharge–charge measurements were carried out at a current density of 200 mA g^{-1} up to 200 cycles in ambient condition. Figure 4b presents the discharge–charge voltage profiles of the carbon-coated TiO_2@Fe_2O_3 electrode. During the first discharge process, there are two apparent voltage plateaus appearing at 0.6 and 1.2 V respectively, which is in good agreement with the CV results. The initial discharge and charge capacities are around 840 and 640 mAh g^{-1}, respectively, corresponding to an irreversible capacity loss of around 27%, which is common for metal-oxide based electrodes.[7,9,11] To show the stability of the electrode, discharge–charge voltage profiles of the 100th and 200th cycles are also presented in Figure 4b. As can be seen, the capacity of the electrode in the 200th cycle is higher than in the 100th cycle and nearly approaches the capacity of the 2nd cycle, indicating good cycling stability.

The cycling performance of the samples is depicted in Figure 4c. For comparison, the data of the pristine TiO_2 nanotube array [obtained by immersing the nanowire sample in mild HCl solution to etch away the $Co_2(OH)_2CO_3$ core, Figure 3d] and a TiO_2@Fe_2O_3 core–shell nanoarray without carbon coating are also presented. The pristine TiO_2 nanotube electrode only delivers a very low capacity with its initial discharge and charge capacity around 265 and 179 mAh g^{-1}, respectively. However, it shows excellent cycling stability. Even after 200 cycles, the TiO_2 nanotube electrode could still deliver a capacity of around 120 mAh g^{-1}. The TiO_2@Fe_2O_3 hollow nanoarray electrode on the one hand has initial discharge and charge capacities that are nearly 3 times that of a pristine TiO_2 nanotube; on the

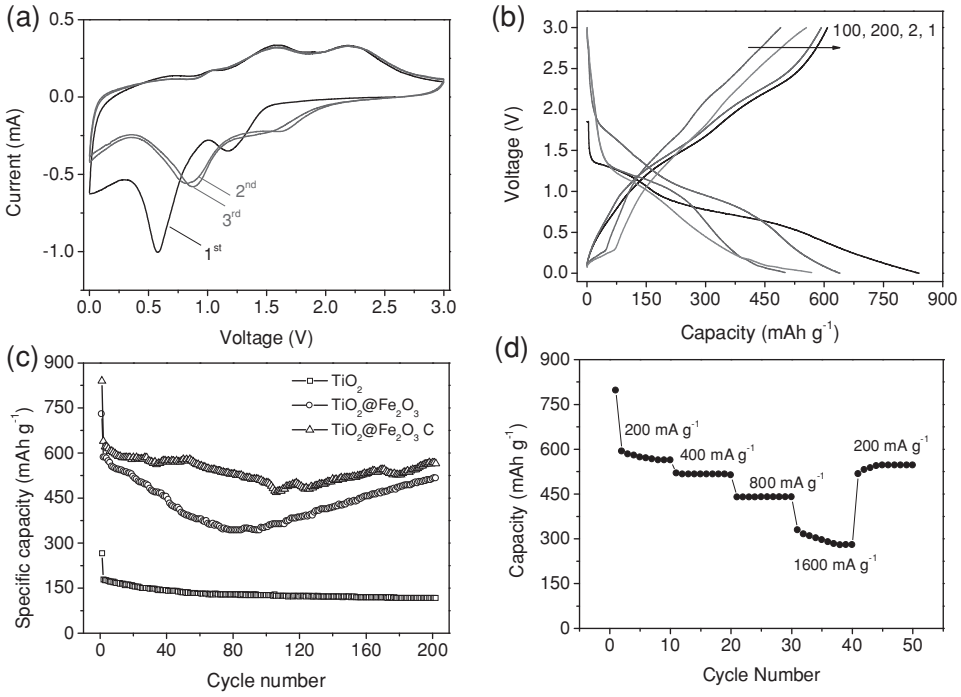

Figure 4. Lithium-ion battery electrode performance. a) CV curves of the TiO_2@Fe_2O_3 electrode at a scan rate of 0.1 mV s^{-1}. b) Galvanostatic discharge/charge profiles of a carbon-coated TiO_2@Fe_2O_3 electrode at a constant current density of 200 mA g^{-1}. c) Cycling performance of the electrodes at a constant current density of 200 mA g^{-1}. d) Rate capability of a carbon-coated TiO_2@Fe_2O_3 electrode at different current densities.

other hand it suffers from degradation. As seen from Figure 4c, the capacity of the TiO_2@Fe_2O_3 electrode first decreases for the initial 90 cycles and then increases for following cycles, giving a high energy capacity of 516 mAh g^{-1} after 200 cycles. This phenomenon is not uncommon for various nanostructured metal-oxide electrodes.[42–44] During the cycling process, the decomposition of the electrolyte may form a coating layer around the active materials to ensure mechanical cohesion, which delivers excess capacity at low potential through a so-called "pseudo-capacitance-type behavior".[45] Another possible reason is the presence of Fe nanoparticles at the TiO_2/Fe_2O_3 interface caused by some irreversible electrochemical reaction, which in turn may improve the reversibility reaction of the active material and result in enhanced capacity.[28] After the carbon encapsulation, the cyclic stability as well as capacity both increase as compared to the bare TiO_2@Fe_2O_3 electrode, which is a result of the structural integrity and improved conductivity.

In addition to the cycling performance, the high-rate capability is another important parameter for LIB application, especially for high-power batteries. As can be seen from Figure 4d, the carbon-coated TiO_2@Fe_2O_3 electrode exhibits a reasonably good cycling response at various current rates. Even when the current reaches 1600 mA g^{-1} the electrode can still maintain a capacity of around 300 mAh g^{-1}. Such outstanding performance is a manifesto of the advantages of our rationally designed hollow hierarchical nanostructures, in addition to the excellent stability of TiO_2 and the presence of carbon.

The structural integrity after repeated cycling is a major issue in rechargeable lithium batteries. To check this, both the impedance and microstructure of the electrode were evaluated after 200 cycles. The electrochemical impedance spectra of the TiO_2@Fe_2O_3 electrode and carbon-coated TiO_2@Fe_2O_3 electrode are interpreted in terms of Nyquist plots as shown in **Figure 5**a. Each plot consists of a semicircle in the high-frequency region and a sloping line in the low-frequency region which are attributed to the charge-transfer process and the mass transfer of lithium ions, respectively.[5] The charge-transfer resistance of the pristine TiO_2@Fe_2O_3 electrode is around 150 Ω. After carbon coating, the resistance decreases to about 77 Ω, indicating a better conductivity. The charge-transfer resistance after cycling is further decreased to around 57 Ω, which might be due to the formation of Fe nanoparticles after irreversible reactions. As for the morphology change, SEM and TEM images of the carbon-coated TiO_2@Fe_2O_3 electrode after 200 cycles are shown in Figure 5b. As can be seen, the electrode retains its one-dimensional hierarchical nanoarray architecture after 200 cycles. Although the Fe_2O_3 nanospikes are pulverized into nanoparticles due to repeated lithiation and delithiation, they are still tightly attached to the surface of TiO_2. This is remarkable, in contrast to the usually observed collapse of one-dimensional nanostructured LIB electrodes.[17]

Finally, we comment on the advantages of the rationally designed nanostructure electrode. The remarkable performance of our electrode mainly comes from the hierarchical hollow core–shell nanostructure configuration. First, the uniform coating of TiO_2 by ALD, and the simultaneous crystallization of TiO_2 and conversion of FeOOH to Fe_2O_3 during annealing result in a rigid hollow structure and tight physical contact between the TiO_2 tube and the Fe_2O_3 nanospikes. Second, the open core–shell structure facilitates electrolyte penetration to

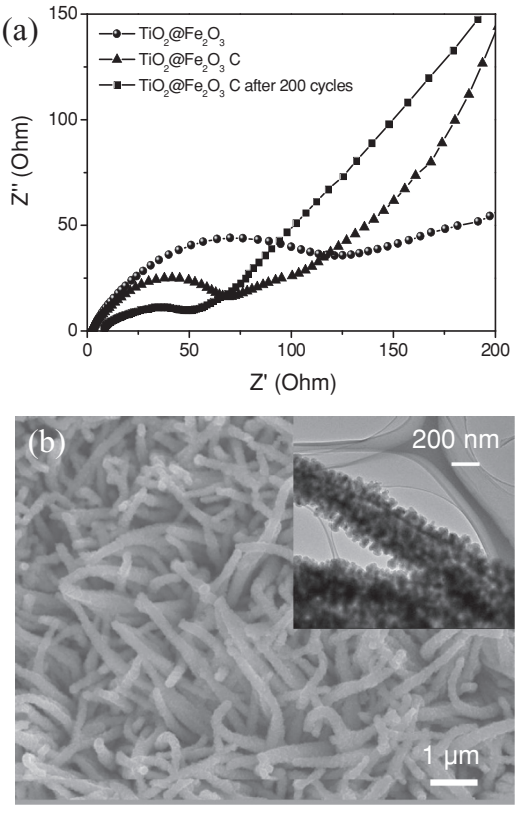

Figure 5. a) Electrochemical impedance spectroscopy of electrodes before and after cycling. b) SEM of the carbon-coated $TiO_2@Fe_2O_3$ electrode after 200 cycles. Inset: TEM image.

every part of the film and thus shortens the diffusion paths for both electrons and lithium ions within the oxides. Last, the overall porous structure provides a larger reaction surface and inner space favoring the efficient contact between the active materials and the electrolyte. This feature provides more active sites for electrochemical reactions and allows facile lithium-ion diffusion at high current density. As a result of these morphological characteristics, the electrode can maintain the enhanced performance up to 200 cycles.

3. Conclusion

We have demonstrated a facile and versatile method to fabricate a $TiO_2@Fe_2O_3$ core–shell nanostructure that combines hollow and hierarchical features with the aid of ALD and a sacrificial $Co_2(OH)_2CO_3$ nanowire template. One stone, two birds: in a single immersion of $Co_2(OH)_2CO_3@TiO_2$ core–shell nanowires into the $FeCl_3$ solution, the nanowire core is replaced with an outer shell of FeOOH and eventually Fe_2O_3, resulting in a hierarchical structure with hollow interior. In such structure, TiO_2 provides not only a stable backbone for the high-capacity Fe_2O_3 nanospikes, but also a conductive path for electrons. As a result, both a higher electrochemical capacity and improved cyclic stability are achieved. As the anode for LIBs, the carbon-coated $TiO_2@Fe_2O_3$ nanostructure exhibit high initial discharge and charge capacities around 840 mAh g^{-1} at a current density of 200 mA g^{-1}. After 200 discharge/charge cycles, the electrode can still deliver a capacity of 530 mAh g^{-1}. We are optimistic that the method demonstrated in this work can be extended to the construction of more complex nanostructures for applications in electrochemical supercapacitors, fuel cells, and solar cells.

4. Experimental Section

Synthesis of $Co_2(OH)_2CO_3$ Nanowire Array: The synthesis of the $Co_2(OH)_2CO_3$ nanowire array on nickel foam was modified from our previous reports.[46] Briefly, $Co(NO_3)_2{\cdot}6H_2O$ (0.6 g), NH_4F (0.15 g), and $CO(NH_2)_2$ (0.6 g) were dissolved in water (70 mL) under magnetic stirring. The resulting solution was then transferred into Teflon-lined stainless steel autoclaves with nickel foam put against the liner wall and it was heated in the electric oven at 105 °C for 5 h. In order to get a good contact, polytetrafluoroethylene tape was uniformly attached to the back side of the nickel foam to inhibit nanowire growth. Note that the exact phase of the obtained nanowires is $Co(CO_3)_{0.5}(OH)0.11H_2O$, according to XRD analysis. For simplicity, it is termed as $Co_2(OH)_2CO_3$ throughout this paper.

Preparation of Hierarchical Hollow $TiO_2@Fe_2O_3$ Core–Shell Nanostructure: The obtained $Co_2(OH)_2CO_3$ nanowire array was coated with a layer of TiO_2 (thickness ca. 10 nm) by ALD (Beneq TFS 200) using $TiCl_4$ and H_2O as the Ti and O precursors, respectively. After that, the nanowire array was immersed into $FeCl_3$ aqueous solution (20 mM) at room temperature for 12 h. By annealing in Ar atmosphere at 400 °C for 2 h, FeOOH transformed to α-Fe_2O_3, and the hierarchical hollow $TiO_2@Fe_2O_3$ core–shell nanostructure was formed. The carbon-coated $TiO_2@Fe_2O_3$ nanostructure resulted by immersing the previous structure into 20 mM glucose solution at room temperature for 24 h, followed by annealing in Ar atmosphere at 400 °C for 2 h.

Structure and Morphology Characterization: The morphology of the as-prepared nanostructures was characterized both by field-emission scanning electron microscopy (FESEM, JEOL JSM 6700F) and transmission electron microscopy (TEM, JEOL JEM-2010). X-ray photoelectron spectroscopy (XPS) measurements were performed using a VG ESCALAB 220i-XL system with a monochromatic Al K_{a1} source (1486.6 eV). All XPS spectra were obtained in the constant pass energy (CPA) mode. The pass energy of the analyzer was set to be 10 eV to ensure high measurement accuracy. The binding energy scale was calibrated with pure Au, Ag, and Cu by setting the Au $4f_{7/2}$, Ag $3d_{5/2}$, and Cu $2p_{3/2}$ binding energies at 83.98, 368.26, and 932.67 eV, respectively.

Electrochemical Performance Test: Standard CR2032-type coin cells were assembled in an Ar-filled glovebox (Mbraun, Unilab, Germany) by directly using the as-fabricated nanostructures on Ni foam as the anode, a Li-metal circular foil (0.59 mm thick) as the counter electrode, and a microporous polypropylene membrane as the separator. The electrolyte consisted of 1 M $LiPF_6$ in ethylene carbonate (EC) and diethyl carbonate (DEC) (1:1, v/v). The cells were aged for 10 h before the measurements. Galvanostatic discharge–charge experiments were performed at different current densities in the voltage range of 0.01–3.00 V with a multichannel battery tester (Neware, China). Cyclic voltammetry (CV) and electrochemical impedance spectroscopy (EIS) were measured by the electrochemical workstation (CHI760D, Chenhua, Shanghai).

Supporting Information

Supporting Information is available from the Wiley Online Library or from the author.

Acknowledgements

This research was supported by SERC Public Sector Research Funding (Grant number 1121202012), Agency for Science, Technology, and Research (A*STAR).

Received: November 19, 2012
Revised: December 12, 2012
Published online: February 18, 2013

[1] P. L. Taberna, S. Mitra, P. Poizot, P. Simon, J. M. Tarascon, *Nat. Mater.* **2006**, *5*, 567.
[2] M. Armand, J. M. Tarascon, *Nature* **2008**, *451*, 652.
[3] P. Poizot, F. Dolhem, *Energy Environ. Sci.* **2011**, *4*, 2003.
[4] B. Dunn, H. Kamath, J.-M. Tarascon, *Science* **2011**, *334*, 928.
[5] Y. Luo, J. Luo, J. Jiang, W. Zhou, H. Yang, X. Qi, H. Zhang, H. J. Fan, D. Y. W. Yu, C. M. Li, T. Yu, *Energy Environ. Sci.* **2012**, *5*, 6559.
[6] Z. Wang, L. Zhou, X. W. Lou, *Adv. Mater.* **2012**, *24*, 1903.
[7] Y. Li, B. Tan, Y. Wu, *Nano Lett.* **2007**, *8*, 265.
[8] B. Varghese, M. V. Reddy, Z. Yanwu, C. S. Lit, T. C. Hoong, G. V. Subba Rao, B. V. R. Chowdari, A. T. S. Wee, C. T. Lim, C.-H. Sow, *Chem. Mater.* **2008**, *20*, 3360.
[9] J. Chen, L. Xu, W. Li, X. Gou, *Adv. Mater.* **2005**, *17*, 582.
[10] C. Kim, M. Noh, M. Choi, J. Cho, B. Park, *Chem. Mater.* **2005**, *17*, 3297.
[11] P. Poizot, S. Laruelle, S. Grugeon, L. Dupont, J. M. Tarascon, *Nature* **2000**, *407*, 496.
[12] S. Yang, Y. Sun, L. Chen, Y. Hernandez, X. Feng, K. Müllen, *Sci. Rep.* **2012**, *2*, 427.
[13] M. V. Reddy, T. Yu, C. H. Sow, Z. X. Shen, C. T. Lim, G. V. Subba Rao, B. V. R. Chowdari, *Adv. Funct. Mater.* **2007**, *17*, 2792.
[14] B. Wang, J. S. Chen, H. B. Wu, Z. Wang, X. W. Lou, *J. Am. Chem. Soc.* **2011**, *133*, 17146.
[15] J. M. Tarascon, M. Armand, *Nature* **2001**, *414*, 359.
[16] J. Liu, Y. Li, H. Fan, Z. Zhu, J. Jiang, R. Ding, Y. Hu, X. Huang, *Chem. Mater.* **2009**, *22*, 212.
[17] Y.-M. Lin, P. R. Abel, A. Heller, C. B. Mullins, *J. Phys. Chem. Lett.* **2011**, *2*, 2885.
[18] A. S. Arico, P. Bruce, B. Scrosati, J.-M. Tarascon, W. van Schalkwijk, *Nat. Mater.* **2005**, *4*, 366.
[19] D. Larcher, C. Masquelier, D. Bonnin, Y. Chabre, V. Masson, J.-B. Leriche, J.-M. Tarascon, *J. Electrochem. Soc.* **2003**, *150*, A133.
[20] J. Jiang, Y. Li, J. Liu, X. Huang, C. Yuan, X. W. Lou, *Adv. Mater.* **2012**, *24*, 5166.
[21] C. Jiang, E. Hosono, H. Zhou, *Nano Today* **2006**, *1*, 28.
[22] X. Lai, J. E. Halpert, D. Wang, *Energy Environ. Sci.* **2012**, *5*, 5604.
[23] X. W. Lou, L. A. Archer, Z. Yang, *Adv. Mater.* **2008**, *20*, 3987.
[24] H. Zhang, X. Yu, P. V. Braun, *Nat. Nano* **2011**, *6*, 277.
[25] A. Magasinski, P. Dixon, B. Hertzberg, A. Kvit, J. Ayala, G. Yushin, *Nat. Mater.* **2010**, *9*, 353.
[26] Z. Wang, D. Luan, S. Madhavi, Y. Hu, X. W. Lou, *Energy Environ. Sci.* **2012**, *5*, 5252.
[27] X. Zhu, Y. Zhu, S. Murali, M. D. Stoller, R. S. Ruoff, *ACS Nano* **2011**, *5*, 3333.
[28] H. Wang, D. Ma, X. Huang, Y. Huang, X. Zhang, *Sci. Rep.* **2012**, *2*, 701.
[29] M. Wagemaker, G. J. Kearley, A. A. van Well, H. Mutka, F. M. Mulder, *J. Am. Chem. Soc.* **2002**, *125*, 840.
[30] J. S. Chen, Y. L. Tan, C. M. Li, Y. L. Cheah, D. Luan, S. Madhavi, F. Y. C. Boey, L. A. Archer, X. W. Lou, *J. Am. Chem. Soc.* **2010**, *132*, 6124.
[31] D. Deng, M. G. Kim, J. Y. Lee, J. Cho, *Energy Environ. Sci.* **2009**, *2*, 818.
[32] Y. Ren, Z. Liu, F. Pourpoint, A. R. Armstrong, C. P. Grey, P. G. Bruce, *Angew. Chem. Int. Ed.* **2012**, *51*, 2164.
[33] J. Luo, S. K. Karuturi, L. Liu, L. T. Su, A. I. Y. Tok, H. J. Fan, *Sci. Rep.* **2012**, *2*, 451.
[34] M. N. Liu, X. L. Li, S. K. Karuturi, A. I. Y. Tok, H. J. Fan, *Nanoscale* **2012**, *4*, 1522.
[35] J. Lee, J. Y. Jho, *Sol. Energy Mater. Sol. Cells* **2011**, *95*, 3152.
[36] A. P. Grosvenor, B. A. Kobe, M. C. Biesinger, N. S. McIntyre, *Surf. Interface Anal.* **2004**, *36*, 1564.
[37] H. Ni, Y. Ni, Y. Zhou, J. Hong, *Mater. Lett.* **2012**, *73*, 206.
[38] X. Liu, J. Zhang, S. Wu, D. Yang, P. Liu, H. Zhang, S. Wang, X. Yao, G. Zhu, H. Zhao, *RSC Adv.* **2012**, *2*, 6178.
[39] W.-M. Zhang, X.-L. Wu, J.-S. Hu, Y.-G. Guo, L.-J. Wan, *Adv. Funct. Mater.* **2008**, *18*, 3941.
[40] J. Liu, Y. Li, R. Ding, J. Jiang, Y. Hu, X. Ji, Q. Chi, Z. Zhu, X. Huang, *J. Phys. Chem. C* **2009**, *113*, 5336.
[41] D. Larcher, D. Bonnin, R. Cortes, I. Rivals, L. Personnaz, J.-M. Tarascon, *J. Electrochem. Soc.* **2003**, *150*, A1643.
[42] T. Zhu, J. S. Chen, X. W. Lou, *J. Phys. Chem. C* **2011**, *115*, 9814.
[43] H.-X. Zhang, C. Feng, Y.-C. Zhai, K.-L. Jiang, Q.-Q. Li, S.-S. Fan, *Adv. Mater.* **2009**, *21*, 2299.
[44] C. Ban, Z. Wu, D. T. Gillaspie, L. Chen, Y. Yan, J. L. Blackburn, A. C. Dillon, *Adv. Mater.* **2010**, *22*, E145.
[45] S. Laruelle, S. Grugeon, P. Poizot, M. Dollé, L. Dupont, J.-M. Tarascon, *J. Electrochem. Soc.* **2002**, *149*, A627.
[46] X. Xia, J. Tu, Y. Zhang, X. Wang, C. Gu, X.-b. Zhao, H. J. Fan, *ACS Nano* **2012**, *6*, 5531.